PCCP

Accepted Manuscript

ROYAL SOCIETY OF CHEMISTRY

www.rsc.org/pccp

Gd(III)-Gd(III) EPR distance measurements – the range of accessible distances and the impact of the zero field splitting

Arina Dalaloyan[1,#], Mian Qi[2,#], Sharon Ruthstein[3], Shimon Vega[1], Adelheid Godt[2,*], Akiva Feintuch[1,*], Daniella Goldfarb[1,*]

[1]Department of Chemical Physics, Weizmann Institute of Science, Rehovot, Israel 76100,
[2]Bielefeld University, Faculty of Chemistry and Center for Molecular Materials, D-33615 Bielefeld, Germany,
[3]Department of Chemistry, Faculty of Exact Sciences, Bar-Ilan University, Ramat Gan, Israel. 5290002

Corresponding authors: Daniella Goldfarb (Daniella.Goldfarb@weizmann.ac.il), Akiva Feintuch (Akiva.Feintuch@Weizmann.ac.il), Adelheid Godt (godt@uni-bielefeld.de)

# Equal contributions. Ms. Dalaloyan carried out all EPR measurements and did the data analysis. Mr. Qi designed and synthesized the compounds used in this study.

Abstract

Gd(III) complexes have emerged as spin labels for distance determination in biomolecules through Double-Electron-Electron Resonance (DEER) measurements at high fields. For data analysis the standard approach developed for a pair of weakly coupling spins with S = ½ was applied and therefore the actual properties of Gd(III) ions, S = 7/2 and ZFS (zero field splitting) ≠ 0, were disregarded. This paper reports on a careful investigation on the consequences of this approach together with the range of distances accessible by DEER with Gd(III) complexes as spin labels.

The experiments were performed on a series of specifically designed and synthesized Gd-rulers (Gd-PyMTA–spacer–Gd-PyMTA) covering Gd-Gd distances of 2-8 nm, which were dissolved in D_2O/glycerol-d_8 (0.03-0.10 mM solutions), i.e. the solvent used for the corresponding experiments on biomolecules. Q- and W-band DEER measurements followed by data analysis using the standard data analysis approach gave distance distribution curves of which the absolute maxima agree very well with the expected distances. However, in case of the short distances of 2.1 and 2.9 nm the distance distributions revealed additional peaks as a consequence of neglecting the pseudo-secular term in the dipolar Hamiltonian during the data analysis, as is outlined in a theoretical treatment. At distances of 3.4 nm and above, negligence of the pseudo-secular term leads to a broadening of max. 0.4 nm of the distance distribution curves at half height. Distances up to 8.3 nm were determined andthe long evolution time of 16 μs at 10 K indicates that a distance of up to 9.4 nm will be determinable. A large distribution of D, as is given for most Gd(III) complexes in a frozen solution, is crucial for the application of Gd(III) complexes as spin labels for distance determination via Gd(III)-Gd(III) DEER, especially for short distances. The larger ZFS of Gd-PyMTA in comparison to that of Gd-DOTA makes Gd-PyMTA a better label for short distances.

Introduction

The distance determination between two well defined sites of a biomolecule, such as a protein or a nucleic acid, using EPR pulse dipolar spectroscopic methods in general and DEER (Double Electron Electron Resonance) in particular, are nowadays well established ways to obtain important information on the structure and conformational space of the biomolecule in frozen solutions.[1-4] Having a straightforward and reliable method for the extraction of the distance distribution[5, 6] from the experimental results has been of major importance for the establishment of such measurements. As the large majority of biomolecules is diamagnetic the EPR approach relies on attaching spin labels at selected sites to the biomolecule.[7,8, 9] The commonly used spin labels are nitroxyl radicals[10,9] introduced in the 1960's,[11] which perform very well as spin labels for DEER measurements at X-band frequencies (~9.5 GHz) and, because of the considerably higher sensitivity, even better at Q-band frequencies (~32 GHz).[12-14] Beyond Q-band frequencies, where further sensitivity increase is expected,[15, 16] the performance of nitroxyl radicals as spin labels is compromised by orientation selection that complicates data analysis.[17, 18] Very recently the trityl radical was introduced as a spin label for proteins and DNA.[19, 20] It features a very narrow EPR spectrum and a long enough phase memory time that allows for room temperature distance measurements on immobilized biomolecules using the DQC (double quantum coherence) pulse sequence.

In the last few years Gd(III) complexes have been introduced as spin labels for distance determination via Gd(III)-Gd(III) DEER at W band (95 GHz) and Ka band (~30 GHz).[21] The use of Gd(III) spin labels features high sensitivity at these frequencies, abolishes orientation selection, and permits shorter pulses and rapid signal averaging. Gd(III)-Gd(III) DEER was demonstrated with model compounds,[22, 23] DNA,[24] proteins,[25, 26] a protein oligomer,[27] a peptide in solution,[28] peptides spanning a lipid bilayer membrane,[29] and gold nanoparticles.[30] Recently, the application of Gd(III) complexes for *in-cell* measurements was demonstrated with Gd(III) spin labeled protein[31] and peptide[32] and the Gd(III) complex Gd-PyMTA was proven to be resistant against reduction within the reducing environment of the cell,[32] quite in contrast to nitroxyl

radicals that become rapidly reduced.[33-35] Most recently a method to further increase the sensitivity of Gd(III)-Gd(III) DEER measurements was reported[36] and it was shown that Gd-Gd distances can be determined using the single frequency RIDME sequence.[37] Furthermore, Gd(III) complexes were used in combination with nitroxyl radicals for distance determination.[38-42]

All mentioned Gd(III)-Gd(III) DEER data were analyzed under the assumption that a Gd(III)-Gd(III) pair can be treated like a pair of nitroxyl radicals[22] and therefore DeerAnalysis,[6] a software package that was developed for a pair of weakly coupling spin labels with S = 1/2, can be used although Gd(III) has S = 7/2 and an associated significant zero field splitting (ZFS). Indeed, the obtained distance distributions were in good agreement with the ones expected based on the results of X-ray analysis,[43] NMR spectroscopy,[25, 26] molecular dynamic simulations,[24] or, in the case of the trans-membrane peptides, simple molecular modeling[29] when taking into account the conformational flexibility of the tether between the Gd(III) ion and the point of label attachment at the molecule of interest. In all cases this flexibility generated a rather broad distance distribution. The applicability of the data analysis approach used was indicated by the result of a Gd(III)-Gd(III) DEER measurement of the model compound **1_1ref** (For the structural formula see Figure 1.) with a well-defined Gd-Gd distance.[22] The distance distribution curve shows a maximum at 2.0 nm which is in good agreement with the Gd-Gd distance determined with X-ray structure analysis on single crystals.[22, 43] Nonetheless, two observations were noted: The modulations were damped as compared to those of nitroxyl-nitroxyl pairs exhibiting the same distance and the modulation depth was lower than expected. Additionally, the distance distribution appeared as too broad when considering the stiffness of the spacer between the two Gd(III) ions. The cause of these unexpected findings may be, as has been suggested earlier,[22, 23] the inappropriateness of the assumption of weak coupling, an assumption that neglects the effects of the dipolar pseudo-secular term in the analysis

As the above mentioned experiments show, Gd(III)-Gd(III) DEER is a very valuable addition to the structure analysis toolbox. Therefore, it is important to know the range of accessible distances and the limits of data analysis with the standard DeerAnalysis

program, i.e. data analysis with the approximation of S = 1/2, with the assumption of weak coupling, and with neglecting the zero field splitting (ZFS). To accomplish this, a series of water soluble model compounds of the type Gd-spacer-Gd, the Gd-rulers $\mathbf{1_n}$ and $\mathbf{2_n}$ (Figure 1), that cover a Gd-Gd distance range from about 2.1-8.5 nm (expected distances) were synthesized. Shock-frozen solutions of these Gd-rulers in a mixture of D_2O and glycerol-d_8 were subjected to DEER measurements at W-band and Q-band frequencies. The data analysis with the standard DeerAnalysis program gave for the Gd-rulers with measured Gd-Gd distances of 3.4 to 8.3 nm distance distributions with a single major peak and occasionally small peaks, the latter being primarily attributed to signal to noise ratio (SNR) limitations and uncertainty in background removal. However, at 2.9 nm and below the distance distributions clearly show artifacts that are caused by neglecting the pseudo-secular term in the dipolar Hamiltonian during the data analysis. As theoretical analysis reveals, the weak coupling condition is not necessarily fulfilled, even if the pump and observer pulses are set apart by as much as 100 MHz, because the central transitions, $|-1/2\rangle \rightarrow |1/2\rangle$, of the two coupled Gd(III) ions overlap. The degree of overlap is a function of the ZFS parameter D and its distribution. The calculations show that the large distribution of D found for many Gd(III) complexes in frozen solutions is crucial for their successful application as general purpose spin labels for distance measurements at Q-band and higher frequencies.

The paper is organized as follows: We first present general EPR characteristics of the Gd-rulers, followed by the results of the DEER measurements and their analysis ignoring the presence of the dipolar pseudo-secular term and the ZFS. In the next section we present a theoretical approach that provides the frequency domain dipolar spectrum of a Gd(III)-Gd(III) pair when taking into account the ZFS interaction through perturbation theory and the pseudo-secular term of the dipolar Hamiltonian by exact diagonalization. The dipolar spectra of the Gd-rulers simulated by using this theory are then presented. We end with a discussion on the implication of the experimental and theoretical findings.

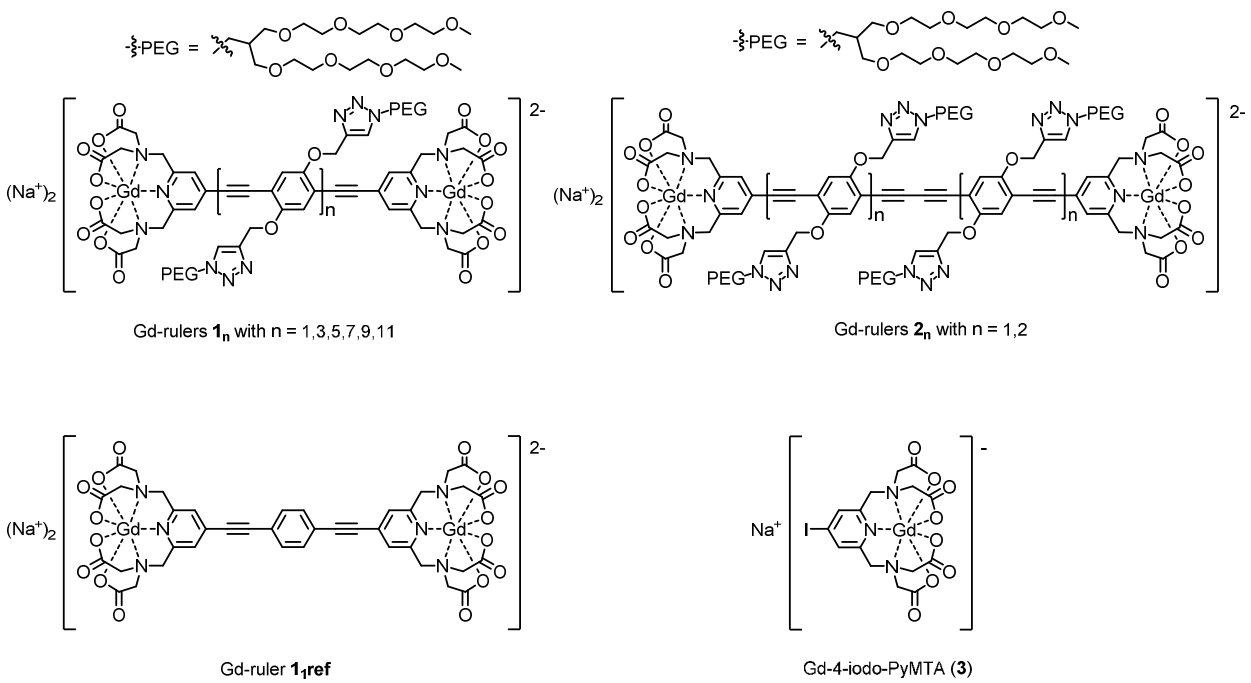

Figure 1. Structural formulae of the compounds used in the herein reported study: Gd-rulers $\mathbf{1}_n$ and $\mathbf{2}_n$, and the parent Gd(III) complex, Gd-4-iodo-PyMTA (**3**). The additionally displayed Gd-ruler $\mathbf{1}_1$**ref** had been used in an earlier study on Gd(III)-Gd(III) DEER.[22] It is structurally identical with Gd-ruler $\mathbf{1}_1$ except for the side chains.

Experimental

Sample preparation

The syntheses of Gd-spacer-Gd $\mathbf{1}_n$ and $\mathbf{2}_n$ (referred to in the text as Gd-rulers) will be reported elsewhere. Stock solutions of Gd-rulers $\mathbf{1}_n$ and Gd-rulers $\mathbf{2}_n$ in water were diluted with a 7:3 (volume ratio) mixture of D_2O and glycerol-d_8 to obtain solutions of the Gd-rulers with the concentrations given in Table S1. Likewise, solutions of Gd-4-iodo-PyMTA (**3**) with the final concentrations being 0.05, 0.10, 0.15, and 0.20 mM were prepared. The stock solutions contained not only the Gd(III) complexes but also NaCl and in case of Gd-ruler $\mathbf{2}_1$ and Gd-4-iodo-PyMTA (**3**) trifluoroacetic acid and sodium trifluoroacetate - a consequence of the syntheses. The amounts of these components are given in Table S2.

EPR measurements

W-band measurements were carried out at 10 K using a home built spectrometer[16]

using quartz capillaries (0.64 mm i.d., 0.8 mm o.d) and sample volumes of 2-3 μl. The Q-band measurements were done at 10 K on an Elexsys E580 Bruker, using a Q-band probe with 2 mm o.d. sample access (~10 μl sample). We chose the temperature of 10 K because at W-band it gives an optimal population difference for the |-1/2> and |1/2> levels, namely an intense central transition.[44] The echo decay rate is also temperature dependent, featuring smaller rates at lower temperatures.[21, 45] Similarly, the spin lattice relaxation is longer at lower temperature.[21, 45] Taking all these consideration into account suggests that 10 K is the optimal temperature for W-band measurements.[21] For Q-band the optimal temperature is probably lower.

W-band echo-detected EPR (EDEPR) spectra were recorded using the two pulse echo sequence π/2-τ-π-τ-echo with a length of 30 ns for the π/2 pulse and a length of 60 ns for the π pulse and τ = 550 ns. The pulse lengths were determined using nutation experiments with the magnetic field set to the maximum of the EPR spectrum, where the central transition dominates. The echo decay was recorded using the same sequence but with varying τ (starting from 100 ns) and at magnetic fields corresponding to the maximum of the EPR spectrum and 90 MHz (3.2 mT) upfield. For both experiments a two-step phase cycling (0, π) was applied over the π/2 pulse. For the Q-band measurements (34.05 GHz) the pulse lengths were 40 ns and 80 ns for the π/2 and π pulse, respectively, τ was 400 ns for EDEPR, and the echo decay was measured at the maximum of the EPR intensity.

Simulation of the EDEPR spectrum was carried out using Easyspin routines[46] and a bimodal Gaussian distribution with the Gaussian centres at D and $-D$ and a width of $|D/2|$. E/D is taken from 0 to 1/3 with a probability of $p(E/D) = E/D\text{-}2(E/D)^2$ as described by Raitsimring et al.[47] The different nutation frequencies, arising from different transition probabilities of the various transitions, were taken into account in the sum of the various transitions.

DEER data were recorded using the four-pulse sequence[48] consisting of a (π/2 - τ_1 - π - τ_1 - π - T - echo) sequence at frequency ν_1 and a π pulse at frequency ν_2 positioned at a variable time t after the first of the two π pulses at ν_1. For W-band DEER, t ranged from

τ_1-200 ns to *T*-500 ns. The DEER evolution time is therefore limited by *T*. For Gd-Gd distances up to 6 nm the pump pulse was set to the maximum of the EPR spectrum and the observer pulses 90 MHz or 100 MHz higher. For the DEER measurements on Gd-rulers $\mathbf{1_9}$, and $\mathbf{1_{11}}$ the observer pulses were set to the maximum of the spectrum and the pump pulse 90 MHz higher. The length of the pump pulse, t_{pump}, was 15 ns, the length of the π/2 observer pulse, $t_{observer,\ \pi/2}$, was 15 ns, and the length of the π observer pulse, $t_{observer,\ \pi}$, was 30 ns. The delay time τ_1 was 350 ns and the repetition time was 500 µs. The cavity tuning was set to 94.9 GHz. For the Q-band measurements *t* ranged from τ_1-100 ns to *T*-300 ns. The pulse lengths were set to be t_{pump} = 28 ns, $t_{observer,\ \pi/2}$ = 20 ns, and $t_{observer,\ \pi}$ = 40 ns, τ_1 was 200 ns and the repetition time was 1 ms. The field was set to the maximum of the spectra, 1215.8 T, and $\Delta\nu$ = ν_2-ν_1 was -100 MHz. The experimental conditions for all measurements are summarized in Table S1 in the Supporting Information. For the W-band measurements full transient echo traces where collected for each *t* value in the DEER sequence and the echo integration was carried out after data collection. The integration gate was chosen such to obtain the best SNR. Usually best results were obtained for an integration width equal to echo full width at half height. The same integration width was applied to all transients in a sequence. For the Q-band measurements the integration width was predetermined by a boxcar integrator to be 80 ns.

Optimization of the experimental conditions for W-band measurements was carried out with Gd-ruler $\mathbf{2_1}$. DEER traces were recorded for fixed observer pulse lengths with $t_{observer,\ \pi/2}$ = 20 ns and $t_{observer,\ \pi}$ = 40 ns and a variable length of the *π* pump pulse. The pump pulse was set at the central transition frequency and $\Delta\nu$ was 90 MHz. The results are shown in Figure S1 in the Supporting Information. It shows that the largest modulation depth, λ, for $\Delta\nu$ = 90 MHz, was achieved for t_{pump} = 15 ns. Measurements were also carried out for a fixed pump pulse length of 15 ns and observer *π/2 and π* pulses of different lengths. The best SNR was observed for $t_{observer,\ \pi/2}$ = 20 ns and $t_{observer,\ \pi}$ = 40 ns (Figure S2). We attribute the lower SNR in case of $t_{observer,\ \pi/2}$ // $t_{observer,\ \pi}$ = 12.5 ns // 25 ns and 15 ns // 30 ns to some overlap of the bandwidths of the pump and echo forming observer pulses.

Data analysis was carried out with DeerAnalysis[6] and Tikhonov regularization using the bending point of the L-curve and with the LongDistance software by Christian Altenbach (the program is written in LabVIEW (National Instruments) and can be freely downloaded from the following site: http://www.chemistry.ucla.edu/directory/hubbell-wayne-l). The background decay was fitted as exponential (mostly for short distances) or stretched exponential.

Results

The EPR spectra and phase memory time

The EDEPR spectra of all Gd-rulers are similar and as examples Figures 2 and S3 present the EDEPR spectra of Gd-ruler **1**$_1$ and **1**$_7$ along with the echo decay curves, recorded at W band at 10 K. Most solutions had a concentration of 0.10 mM but not all. For the Gd-rulers with the largest Gd-Gd distances, Gd-rulers **1**$_9$ and **1**$_{11}$, a concentration of 0.05 mM was chosen in order to minimize the background decay so that it will not mask the long modulation period in the DEER measurements. We did not find any correlation between the echo decay rate and the Gd-Gd distance. For example, for 0.10 mM samples of Gd-rulers **1**$_1$ and **1**$_7$ and a field set to the maximum of the EPR spectrum, the echo decayed to 10% of its initial value, $\tau_{10\%}$, within 8.80 and 8.25 μs, respectively (Figure 2). Reducing the concentration of Gd-ruler **1**$_1$ to 0.05 mM and of **1**$_7$ to 0.03 mM prolonged the decay time and $\tau_{10\%}$ increased to 9.10 and 9.19 μs, respectively (Figure S3). When the field is set to + 90 MHz off maximum as compared to being set to the maximum of the spectrum the echo decay is faster (Figure S3), as reported earlier.[45]

A partial Q-band EDEPR spectrum of Gd-ruler **1**$_3$ is shown in Figure 2d and the corresponding echo decay is presented in Figure 2f. In the Q-band echo decay trace ^{2}H modulations from the deuterated solvent are evident. We found that at Q band the echo decay is faster than at W band.

Figure 3 presents the EDEPR spectrum of the parent Gd(III) complex, Gd-4-iodo-PyMTA (**3**). It also shows simulations, carried out as described in the experimental section, yielding D = 1150 MHz. The positions of the pump and observer pulses in the

DEER experiments are given in Figure 3 as well, showing that whereas the pump pulse addresses mostly the central transition, the observer pulses mainly address the |-3/2> → |-1/2> transition.

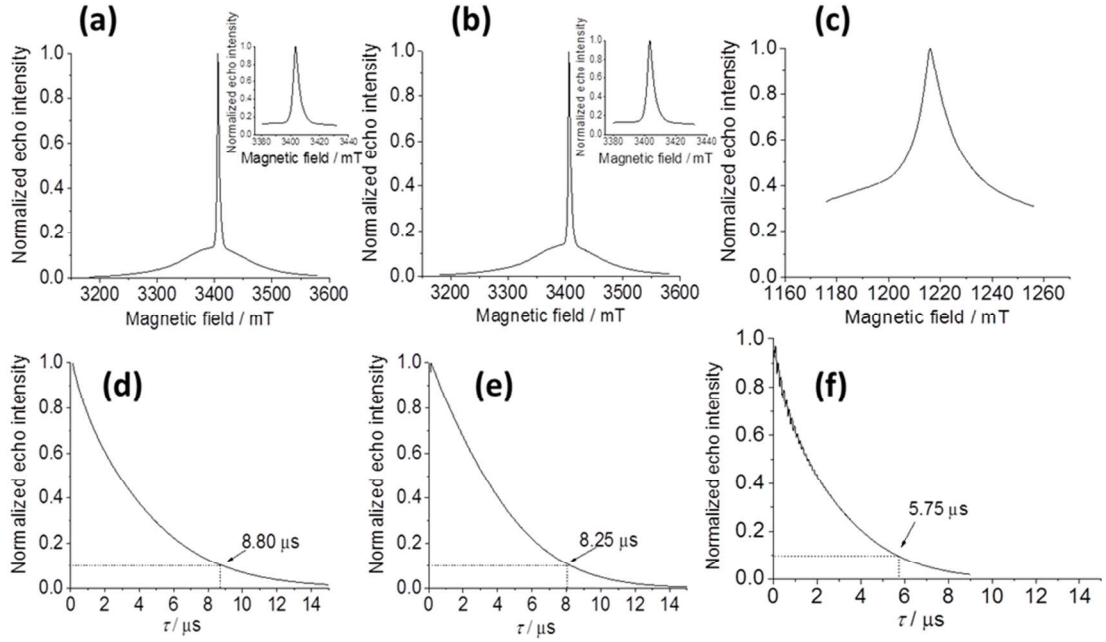

Figure 2. W-band EDEPR spectra of 0.10 mM solutions of (a) Gd-ruler $\mathbf{1_1}$ and (b) Gd-ruler $\mathbf{1_7}$ in D_2O/glycerol-d_8 (7/3, volume ratio). The insets show a blow up of the region of the central transition. (c) Q-band EDEPR spectrum of a 0.10 mM solution of Gd-ruler $\mathbf{1_3}$ in D_2O/glycerol-d_8 (7/3, volume ratio) showing the central transition region. (d,e). W-band echo decay traces corresponding to the spectra shown in panels (a) and (b). (f) Q-band echo decay trace corresponding to the spectrum shown in panel (c). For easy comparison the $\tau_{10\%}$ values are noted on the figures. All measurements were carried out at 10K and the echo decays were measured at a field corresponding to the maximum of the EDEPR spectrum.

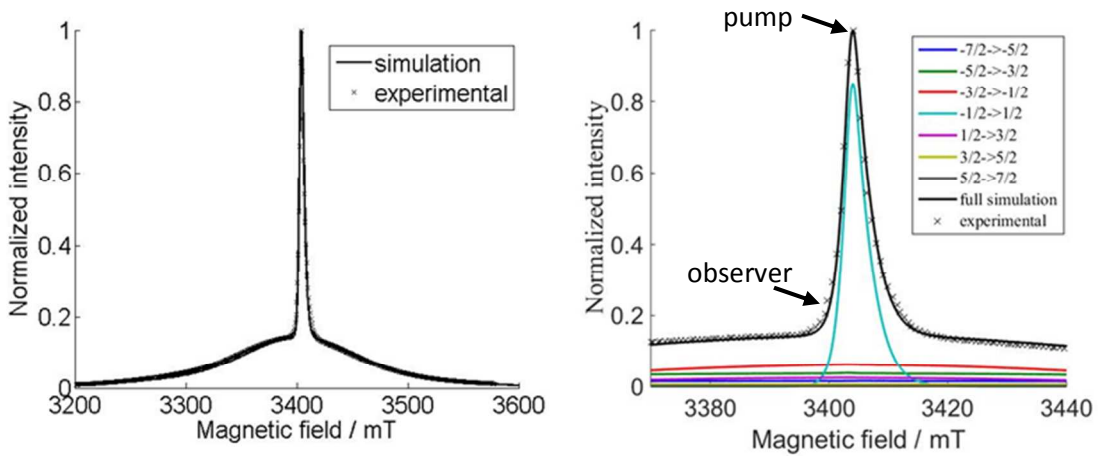

Figure 3. (a)The full W-band EDEPR spectrum of a 0.10 mM solution of Gd-4-iodo-PyMTA (**3**) in D_2O/glycerol-d_8 (7/3, volume ratio) at 10 K (symbols) and the simulations (solid lines) with D = 1150 MHz and a bimodal Gaussian distribution with the Gaussian centres at D and -D and a width of |D/2|. E/D is taken from 0 to 1/3 with a probability of $p(E/D) = E/D\text{-}2(E/D)^2$.[47] (b) A blow-up of the central transition. The simulated spectra show the individual transitions and their sum with the color codes shown in the figure. The positions of the pump and observer pulses are indicated.

DEER results

To confirm that the background decay in the DEER measurements is exponential as expected for a homogenous isotropic solution and to determine the modulation depth λ, we carried out DEER measurements on a series of solutions of the parent Gd(III) complex, Gd-4-iodo-PyMTA (**3**), differing in concentration. All DEER traces (Figure S4a) showed a linear decay which is expected for an exponential decay with a small exponent (small λ). Plotting the decay slopes as a function of concentration gave a linear curve from which the modulation depth λ = 0.052±0.002 was determined (For details see Figure S4b and accompanying text in the Supporting Information). This modulation depth means that only 5.2% of all spins are excited by the pump pulse. The Gd(III) spectrum is a superposition of several transitions, whose relative intensities are temperature and spectrometer frequency dependent. The experimentally determined λ value is a weighted average of individual λ_i values, each corresponding to a different transition.[21] Calculation of λ for Gd(III)-Gd(III) DEER based on the overlap integral

between the pump pulse excitation profile and the echo detected spectrum predicted λ = 7.6%. The experimentally determined value of 5.2% is in reasonable agreement considering that the transition dependence of the nutation frequency was neglected.

The results of W-band DEER measurements on Gd-rulers $\mathbf{1_n}$ and $\mathbf{2_n}$ are shown in Figures 4 and S5 and are summarized in Table 1. The experimental conditions and sample concentrations are given in Table S1. Except for Gd-rulers $\mathbf{1_9}$ and $\mathbf{1_{11}}$, the pump pulse frequency was set to the central transition, which gave a modulation depth of 3-4%. Setting the observer frequency to the central transition, as done in the case of Gd-rulers $\mathbf{1_9}$ and $\mathbf{1_{11}}$, yielded a modulation depth of around 1% (Table 1). Under the latter conditions the measurements are more susceptible to artifacts due to the lower modulation depth and therefore for Gd-Gd distances below 7 nm the pump pulse was set to the central transition. However, for Gd-Gd distances above 7 nm a long evolution time becomes essential and therefore we set the observer pulses to the central transition because the phase memory time is longer for the central transition. A comparison of the DEER traces recorded for Gd-ruler $\mathbf{1_9}$ under both conditions - pump pulse or observer pulses set to the central transition - is shown in Figure S6 and the experimental details and results are given in Table S2.

The Fourier transforms (FT) of the DEER traces are expected to give Pake powder patterns. As Figure 4b shows, Pake patterns were obtained for Gd-rulers with Gd-Gd distances of 3.4 nm and above. However, for shorter distances, such as 1.9 nm (Gd-ruler $\mathbf{1_1}$) and 2.9 nm (Gd-ruler $\mathbf{2_1}$), the FT spectra show severe distortions from the expected Pake pattern. A similar result was found for the structurally closely related Gd-ruler $\mathbf{1_1}$**ref**, a ruler like Gd-ruler $\mathbf{1_1}$, however without side chains (see Figure 1 for the structural formula).[22] The dipolar frequencies, ω_{dd}, obtained from the spectra are listed in Table 1 and the distance distributions, derived using DeerAnalysis and Tikhonov regularization, are given in Figure 4c. The distances corresponding to the absolute maxima of the distance distribution curves are listed in Table 1 together with the expected distances and in Figure 6 the data are plotted against each other. For details on the calculation of the expected distances see the Supporting Information. In all cases, the maximum of the distance distribution is in agreement with the expected distance. However, in case of Gd-rulers $\mathbf{1_1}$ and $\mathbf{2_1}$, that gave distorted Pake patterns,

the major peak at the expected distance is accompanied by minor peaks (shoulders) at larger distances. As discussed in detail in the next section, these artifact peaks arise from the use of the wrong kernel in the extraction of the distance distribution. Ghost peaks appear also for the Gd-rulers $\mathbf{1}_3$ and $\mathbf{2}_2$ with a Gd-Gd distance of 3.4 and 4.3 nm, respectively. When analyzing the DEER data with the LongDistance software the intensity of these ghost peaks diminishes (Figure S7). Therefore, we conclude that they arise from the uncertainty of the background removal in the data analysis and SNR limitations. The width at half height of the distance distributions of all Gd-rulers with a Gd-Gd distance of 3.4 nm and above ranges between 0.4-0.7 nm, with slightly broader distributions as the distance increases. This broadening is at least partially due to insufficient spectral resolution coming from the limited time window.

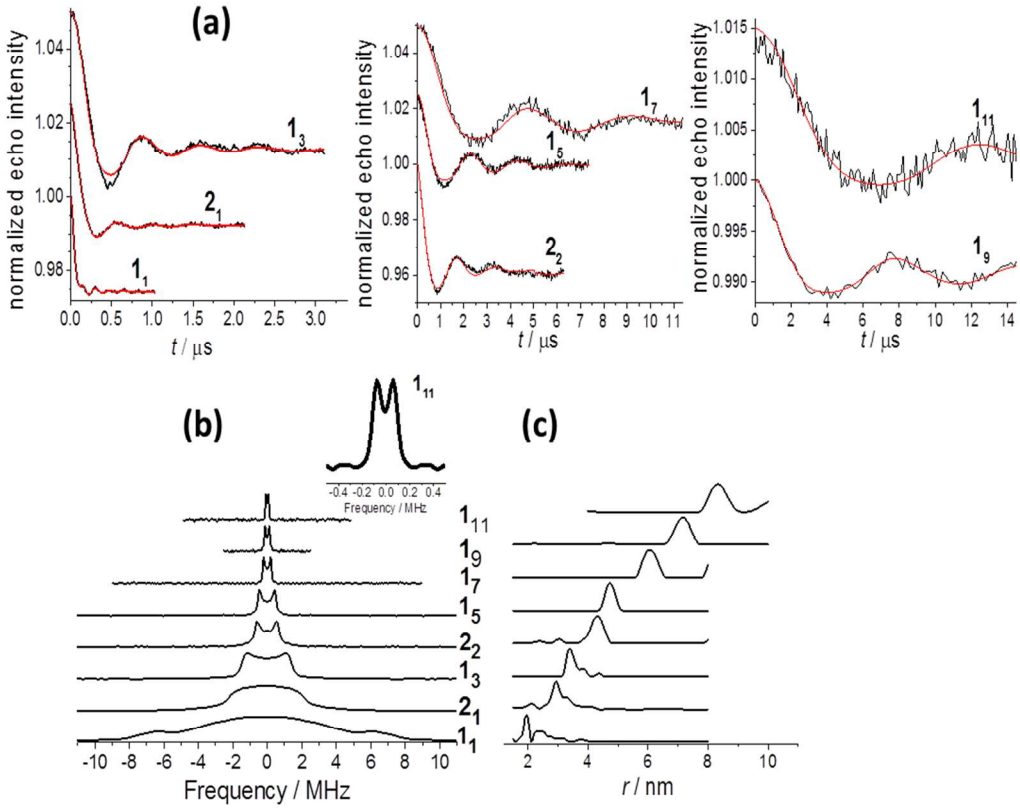

Figure 4. Results of W-band DEER measurements of Gd-rulers $\mathbf{1}_n$ and $\mathbf{2}_n$ in D_2O/glycerol-d_8 (7/3 volume ratio) at 10 K. For experimental details see Table S1. (a) Background corrected DEER traces. (b) FT spectra of the DEER traces shown in panel (a). The inset is a blow-up of the data of Gd-ruler $\mathbf{1}_{11}$. c) Distance distributions obtained by Tikhonov regularization.

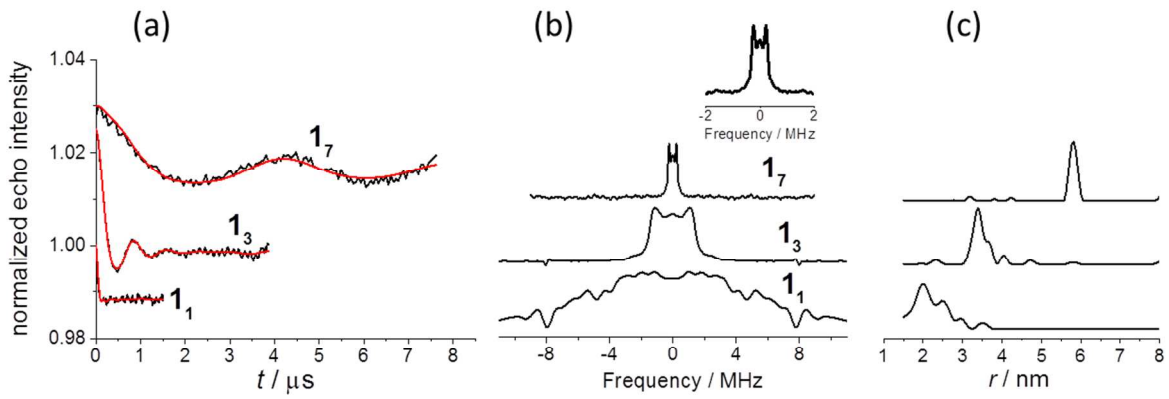

Figure 5. Results of Q-band DEER measurements of Gd-rulers $\mathbf{1}_1$, $\mathbf{1}_3$, and $\mathbf{1}_7$ in D_2O/glycerol-d_8 (7/3 volume ratio) at 10 K. For experimental details see Table S1. (a) DEER traces after background subtraction. (b) FT spectra of the DEER traces shown in panel (a). The inset is a blow up of the spectrum of Gd-ruler $\mathbf{1}_7$. (c) Distance distributions obtained by Tikhonov regularization.

Gd-rulers $\mathbf{1}_1$, $\mathbf{1}_3$, and $\mathbf{1}_7$ were also measured at Q band and the data are shown in Figures 5 and S8. In general there is a very good agreement between W- and Q-band measurements. Also the distortions of the Pake pattern of Gd-ruler $\mathbf{1}_1$ are clearly to be seen, as well as the artifacts in the associated distance distribution. The same was found for the Gd-ruler $\mathbf{1}_1$**ref**.[22] The Q-band dipolar spectra for Gd-rulers $\mathbf{1}_1$ and $\mathbf{1}_3$ show weak signals at about $\pm$ 8 MHz, which are due to ^{2}H modulation.

In the next section we account for the distortions observed in the Pake patterns and distance distributions of the Gd-rulers $\mathbf{1}_1$ and $\mathbf{2}_1$ with Gd-Gd distances of 2.1 and 2.9 nm.

Table 1. Summary of the results of DEER measurements of Gd-rulers $\mathbf{1}_n$ and $\mathbf{2}_n$. The values in the second row correspond to Q-band data, all others to W-band data. The pump pulse was set to the central transition except for the DEER experiments with Gd-rulers $\mathbf{1}_9$ and $\mathbf{1}_{11}$ in which the observer pulse was set to the central transition. The numbers given for the experimentally determined Gd-Gd distances correspond to the absolute maxima of the distance distribution curves. The calculations of the expected Gd-Gd distances were done using experimental data from structurally related nitroxyl-rulers (nitroxyl-spacer-nitroxyl; Figure 6) and the Gd-Gd distance of Gd-ruler $\mathbf{1}_1$**ref** in the crystalline state. For details see the text and the Supporting Information.

Gd-rulers	$\omega_{dip}/2\pi$, MHz[a]	Gd-Gd distance, nm exp. determ.	Gd-Gd distance, nm expected	$\triangle r$, nm [b]	modulation depth λ, %
$\mathbf{1}_1$	6.4	1.9 2.0	2.1	-----	2.5 1.2
$\mathbf{2}_1$	1.7	2.9	3.0	0.3	3.2
$\mathbf{1}_3$	1.1	3.4 3.4	3.4	0.4 0.4	3.9 2.7
$\mathbf{2}_2$	0.57	4.3	4.3	0.5	4.1
$\mathbf{1}_5$	0.42	4.7	4.7	0.5	2.9
$\mathbf{1}_7$	0.19	6.0 5.8	5.9	0.6 0.25	3.3 1.4
$\mathbf{1}_9$	0.11	7.2	7.1	0.6	0.75
$\mathbf{1}_{11}$	0.06	8.3	8.5	0.7	1.1

[a] ω_{dip} is half the splitting between the perpendicular singularities of the Pake pattern.

[b] Full width at half height of the distance distribution main peak.

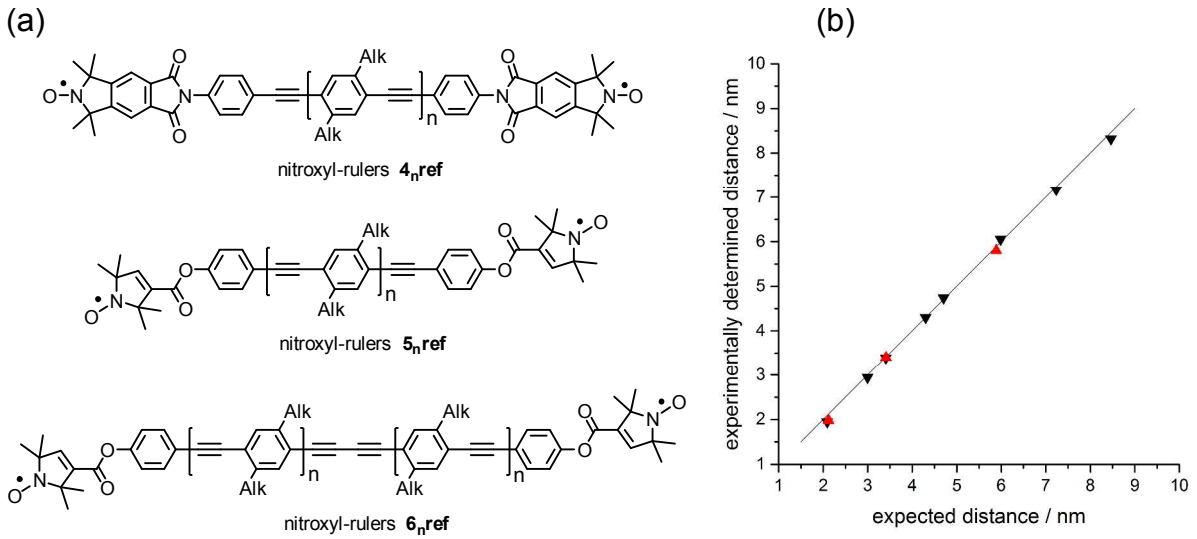

Figure 6. (a) Structural formulae of nitroxyl-rulers **4$_n$ref**-**6$_n$ref** having the same spacers as the Gd-rulers **1$_n$** and **2$_n$**. Alk stands for hexyl as well as for 6-methoxyhexyl. The concrete structural formulae are given in the literature.[49] The results of nitroxyl-nitroxyl DEER measurements on these nitroxyl-rulers served the calculation of the expected Gd-Gd distances. (b) A plot of the distances corresponding to the maxima of the Gd-Gd distance distribution curves of the Gd-rulers **1$_n$** and **2$_n$** obtained in this work versus the expected Gd-Gd distances. The black symbols correspond to W-band data and the red symbols to Q-band data. The solid line indicates where the data points should sit if the experimentally determined and the expected Gd-Gd distances were identical.

Theory

In this section we will describe the special characteristics of a DEER experiment with a pair of Gd(III) ions, i.e. a pair of spins with S = 7/2, as opposed to a DEER experiment with a pair of nitroxyl radicals, i.e. a pair of spins with S = 1/2. We reveal the origin of the deviations in the DEER spectra at short distances from ideal Pake patterns.

The spin Hamiltonian for a pair of electrons with S > 1/2 is given by:

$$H = \sum_{i=1,2} (\omega_{ei} S_{zi} + \overline{S}_i \cdot \overline{\overline{D^i}} \cdot \overline{S}_i) + \overline{S}_1 \cdot \overline{\overline{T}} \cdot \overline{S}_2 \quad (1)$$

where $\overline{\overline{D^i}}$ is the zero field splitting (ZFS) tensor of each of the electrons and T is the electron-electron dipole interaction tensor. In the principal axis of $\overline{\overline{D^i}}$ the ZFS is

represented by the parameters $D_i = 3D_{zz,i}/2; \quad E_i = (D_{xx,i} - D_{yy,i})/2$. Due to the large Zeeman energy at high fields both the ZFS and the dipolar parts of the Hamiltonian can be truncated. For the dipolar interaction only the secular and pseudo-secular terms need to be taken into account. They are given by:

(2) $$H_d^{secular} = \omega_{dip} S_z^1 \, S_z^2 \, (3cos^2\theta_d - 1)$$

$$H_d^{pseudosecular} = -\frac{\omega_{dip}}{4} \, (S_+^1 S_-^2 + S_-^1 S_+^2) \, (3cos^2\theta_d - 1)$$

where $\omega_{dip} = \frac{\mu_B^2 g_1 g_2}{\hbar} \frac{1}{r_{12}^3}$ is the dipolar coupling frequency for an electron-electron distance of r_{12}, and θ_d is the angle between the principal axis system of the dipolar interaction (the vector connecting the two Gd(III) ions) and the external magnetic field.

As we are working at a relatively high field and since in general the ZFS of the Gd(III) complex is small and usually does not exceed 40 mT,[47] we take into account only the first order terms of the ZFS for all transitions given by:

(3) $$H_{ZFS}^{(1)} = \sum_{i=1}^{2} \frac{D^i}{2} (3cos^2\theta_{ZFS}^i - 1)[(S_z^i)^2 - \frac{1}{3}S(S+1)]$$

whereas for the |-1/2>→|1/2> transition a second order contribution is added:[50]

(4) $$H_{ZFS}^{(2)} = -\sum_{i=1}^{2} \frac{(D^i)^2}{\omega_e} [sin^2\theta_{ZFS}^i cos^2\theta_{ZFS}^i [S_z^i (2(S_z^i)^2 + \frac{1}{4}) - S(S+1)]$$

$$+ \frac{1}{4} sin^4\theta_{ZFS}^i [S_z^i ((S_z^i)^2 + \frac{1}{2}) - S(S+1)]]$$

where θ_{ZFS}^i is the angle between the principal axis system of the ZFS and the external magnetic field and where the index *i* refers to each of the Gd(III) ions. In Eqs. (3) and (4) the ZFS is assumed to have an axial symmetry for simplicity.

In order to demonstrate the effect of the dipolar flip-flop term (the pseudo-secular term, Eq. 2) on the result of a Gd(III)-Gd(III) DEER experiment it is necessary to calculate the DEER spectrum for the case of *S* = 7/2 under the conditions similar to those described above, while averaging over θ_d.

Figure 3 discloses the contribution of the individual EPR transitions to the DEER experiment at 95 GHz and 10K. In the following we use the usual notation that spin A is the observed spin, while spin B is the pumped spin. The pump pulse covers a significant part of the |-1/2>→|1/2> transition of spin B while the main contribution to the detected signal is from the |-3/2> → |-1/2> transition of spin A. We will therefore calculate the DEER spectrum assuming spin B is pumped at the |-1/2(B)>→|1/2(B)> transition while spin A is observed at the |-3/2(A)> → |-1/2(A)> neglecting contributions from other transitions. To understand the DEER experiment under these conditions it is helpful to look at the energy level diagram of the system. For simplicity we will demonstrate this point on a model system with $S_A = S_B = 3/2$. The energy level diagram of such a system is shown in Figure 7. The largest level splitting originates from the Zeeman energy depending on $S_z = S_{z,A} + S_{z,B}$. The levels are then additionally split by the ZFS energy

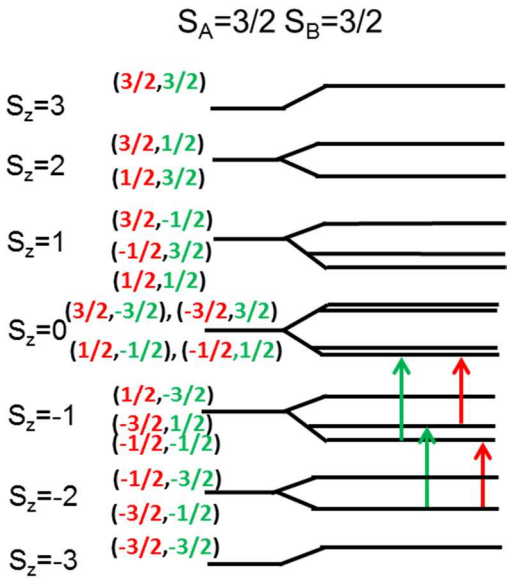

Figure 7. Energy level diagram of a system with S_A = 3/2, S_B = 3/2 demonstrating the positioning of the pump and observer pulse participating in the DEER experiment. The M_S values of spins A and B and their corresponding transitions are given in red and green, respectively.

and by dipolar energies. The DEER effect is a result of the population inversion

between the |-3/2(A),-1/2(B)> and |-3/2(A),1/2(B)> levels and the |-1/2(A),-1/2(B)> and |-1/2(A),1/2(B)> levels due to the pump pulse on spin B, as shown by the green arrows in the Figure. The DEER oscillation frequency is given by the energy difference between two observed transitions, the |-3/2(A),-1/2(B)>→|-1/2(A),-1/2(B)> transition and the |-3/2(A),1/2(B)>→|-1/2(A),1/2(B)>
transition, represented by the red arrows:

$$(5)\quad \omega_{DEER} = \omega_{-3/2_A,-1/2_B \to -1/2_A,-1/2_B} - \omega_{-3/2_A,1/2_B \to -1/2_A,1/2_B}$$

As mentioned previously the contribution of the first order ZFS shift to the energy of the |-1/2(A),1/2(B)> and the |1/2(A),-1/2(B)> states is identical. The energy difference between these two levels is a result of the orientation dependence of the second order ZFS and can be quite small as is illustrated in Figure 7. As a result the off-diagonal dipolar pseudo-secular term is not small relative to the matrix elements that it connects and therefore it needs to be taken into account.

As we will show, diagonalization of the Hamiltonian while taking the pseudo-secular term into account will shift the energy of these two levels. This in turn will shift the |-3/2(A),1/2(B)> → |-1/2(A),1/2(B)> transition energy whereas all other transitions |-3/2(A),χ(B)> → |-1/2(A),χ(B)> are the same for all other $S_{z,B}$ values: χ = [-3/2,-1/2,3/2].

Coming back to the S = 7/2 case, this effect is demonstrated in Figure 8. The figure shows a calculation with exact diagonalization of the |-3/2> → |-1/2> transition of spin A split by the dipolar interaction with spin B as a function of $D_\perp$ =-D/3 . The calculation was done using EasySpin.[46] A large ZFS parameter removes the degeneracy of the |1/2(A),-1/2(B)> and |-1/2(A)1/2(B)> levels and then the dipolar pseudo-secular term can be neglected as it becomes small compared to the energy difference between the states it connects. As $D_\perp$ gets smaller the two levels come together, the dipolar pseudo-secular term becomes significant and the |-3/2(A),1/2(B)>→|-1/2(A),1/2(B)> transition energy is shifted. This will result in a change in the DEER oscillation frequency which, as described above, is given by the energy difference between the |-3/2(A),-1/2(B)>→|-1/2(A),-1/2(B)> transition and the |-3/2(A),1/2(B)>→|-1/2(A),1/2(B)> transition (Eq. 5).

Note that at large $D_\perp$ values another effect sets in, which is due to second order mixing of states due to the ZFS that is manifest by unequal splitting of the multiplet.[21] The higher the magnetic field the smaller is this effect. Namely, this effect is expected to affect significantly X-band measurements and to a lesser extent Q-band measurements. If one observes the central transition, similar shifts will be found for transitions involving $M_s = \pm 1/2$ of spin B.

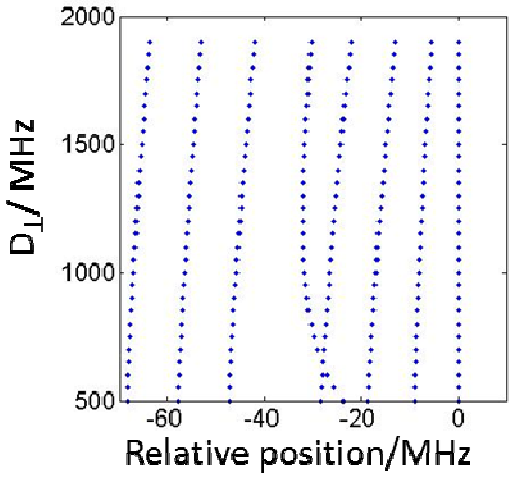

Figure 8. Zoom-in on regions of the |-3/2> → |-1/2> transition of the Gd(III) (A) signals of the 95 GHz EPR spectrum (partial range) for a single orientation of two coupled Gd(III) ions with the same ZFS. The transition energies are shown as a function of $D_\perp$ *(-D/3)* for Gd(III)(A) $\theta^A_{ZFS} = 20^0$ and for Gd(III)(B) $\theta^B_{ZFS} = 80^0$, relative to B_0. The orientation of the dipolar axis is $\theta_d = 20^0$, $\phi_d = 0$ with respect to B_0. The calculations were done for ω_{dip} = 6.0 MHz using EasySpin[46] with exact diagonalization. For simplicity the zero was set at the highest frequency line. The lowest frequency line of the multiplet corresponds to the $M_S = 7/2$ state of Gd(III)(A) and the highest one corresponds to $M_S = -7/2$ of Gd(III)(A). As $D_\perp$ is reduced only the |-3/2(A),1/2(B)>→|-1/2(A),1/2(B)> transition energy (frequency) is significantly shifted as explained in the main text.

Next we present a simplified approach that we used to estimate the shape of the DEER spectrum. The basic idea is that to obtain the DEER frequencies it is necessary to calculate only the energy of the relevant four levels: [|-3/2(A),-1/2(B)>, |-3/2(A),1/2(B)> ,

|-1/2(A),1/2(B)>, |-1/2(A),-1/2(B)>]. The energy of the three levels [|-3/2(A),-1/2(B)>, |-3/2(A),1/2(B)>, |-1/2(A),-1/2(B)>] can be obtained directly from the diagonal elements of the Hamiltonian in Eqn. 1-4 since for these levels all off-diagonal terms can be neglected. The |-1/2(A),1/2(B)> level has a significant off-diagonal term in the [|-1/2(A),1/2(B)>, |1/2(A),-1/2(B)>] subspace and it is therefore necessary to diagonalize this block of the Hamiltonian which for $S_A = S_B = 7/2$ is given by:

(6)

$$\begin{bmatrix} \left(\sum_i (-1)^{i-1}\frac{(D^i)^2}{\omega_e}\left(\frac{15}{2}\cos^2\theta^i_{ZFS}\sin^2\theta^i_{ZFS}-\frac{15}{8}\sin^4\theta^i_{ZFS}\right)\right. & -16\omega_{dip}(3\cos^2\theta_d-1) \\ \left.+\frac{\omega_{dip}}{4}(3\cos^2\theta_d-1)\right) & \\ -16\omega_{dip}(3\cos^2\theta_d-1) & \left(\sum_i (-1)^{i}\frac{(D^i)^2}{\omega_e}\left(\frac{15}{2}\cos^2\theta^i_{ZFS}\sin^2\theta^i_{ZFS}-\frac{15}{8}\sin^4\theta^i_{ZFS}\right)\right. \\ & \left.+\frac{\omega_{dip}}{4}(3\cos^2\theta_d-1)\right) \end{bmatrix}$$

Following the diagonalization we can extract the energy of the |-1/2(A),1/2(B)> level and together with the values for the other three levels obtain the DEER oscillation frequency for a given set of orientations (see eq. 5). To calculate the full powder spectrum we loop independently over the angle set $[\theta^A_{ZFS}, \theta^B_{ZFS}, \theta_d]$ defining the orientations of the two ZFS tensors and the dipolar tensor with respect to the magnetic field. We assume no correlation between them as justified by the large distribution of the ZFS parameters.[47] Here we neglected contributions to the observed spin A signal from transitions other than the |-3/2> → |-1/2> transition, that are small, however not zero.

Calculation of the powder dipolar spectra

The calculations of the dipolar powder spectra were done with a home written Matlab script. Figures 9a,b present the calculated dipolar spectra for two different values of *D* for Gd-Gd distances similar to those of the Gd-rulers $\mathbf{1_1}$ and $\mathbf{2_n}$ used for the experiments. As a first stage we assumed for simplicity that we detect the full bandwidth

of the |-3/2> → |-1/2> transition of spin A. We can clearly see distortions in the Pake pattern as the distances get shorter similar to the distortions found experimentally. The comparison of Figures 9a and 9b shows that with larger *D* the distortions are smaller because the degree of overlap of the central transitions of the two spins is smaller. Because Gd(III) complexes have a large distribution in *D* (Figure 3),[47] we illustrate the effect of the distribution of *D* in Figure 9c.The calculated spectra for Q-band are shown in Fig. S9. We simplified the calculations by assuming an axial ZFS tensor and therefore we did not use the distribution of *D* and *E* used in Figure 3 but limited ourselves to a Gaussian distribution of *D* centered at 1150 MHz with a 1000 MHz bandwidth.

The calculations were done in two steps: (i) We looped over different values of *D* in the range of -2000 MHz < *D* < 2000 MHz. For each value of *D*, we identified the orientations for which the -3/2(A) → -1/2(A) transition falls into the range of the detection window estimated to have a width of 100MHz around the detection frequency positioned 100MHz above the pump such that $\nu_{pump}+50MHz<\nu_{-3/2_A,\pm1/2_B\rightarrow-1/2_A,\pm1/2_B}<\nu_{pump}+150MHz$, . For these orientations the DEER frequencies were calculated according to Eq. 5. (ii) Each DEER frequency calculated in (i) was weighted according to its *D* value using a Gaussian distribution as mentioned above. The full powder spectrum was then calculated as a histogram of DEER frequencies with the proper weighting. The distortions in the Pake pattern increase as the distances get shorter, similar to the distortions seen in the experiment. We conclude that we understand the source of the distortion, and that for distances of 3.4 nm and above, the pseudo-secular term of the dipole-dipole interaction can be neglected. Nonetheless, for distances at 3.4 nm and above some artificial broadening of the Pake pattern, which decreases with increasing distance, is noticeable and this will manifest as an artificial broadening in the distance distribution.

In the calculations presented above, we did not take into account the contributions of the |-5/2> → |-3/2> and |-7/2> → |-5/2> transitions to the observed spin A signal . These do have some finite contributions (see Figure 3) and the dipolar powder pattern they produce are not affected by the pseudo-secular term. This in turn should reduce somewhat the broadening of the Pake patterns shown in Figure 9. All our calculations

are based on the Hamiltonian given in Eq. 1, which did not take account that about 30% of the Gd isotopes that have a nuclear spin of 3/2 (^{155}Gd, 14.80% natural abundance, ^{157}Gd, 15.65 % natural abundance) and should exhibit a small hyperfine coupling.[51] The effect of such an hyperfine coupling term on the applicability of the weak coupling approximation is yet to be explored.

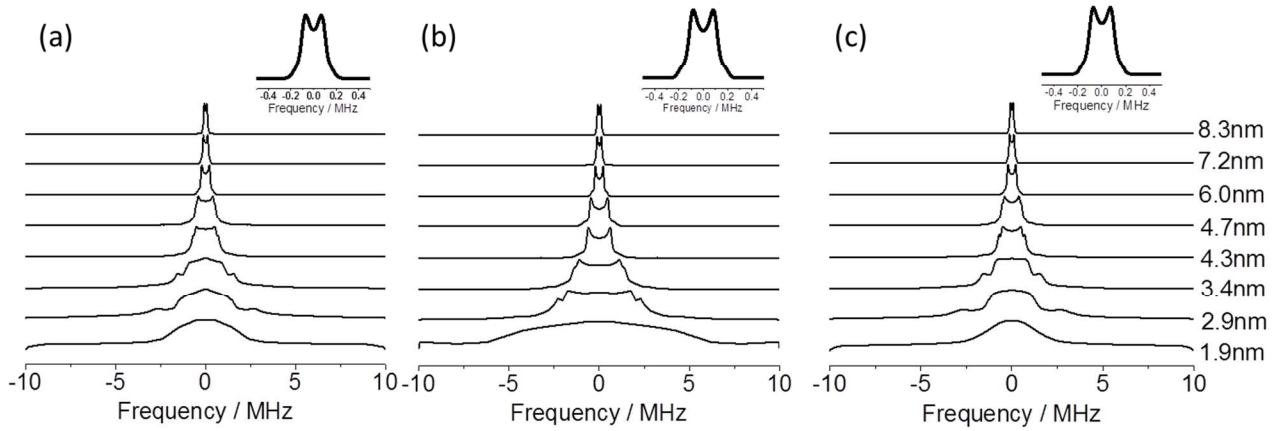

Figure 9. Calculated DEER spectra for Gd-Gd distances similar to the ones measured. The parameters used were (a) D_{ZFS}^{A} = D_{ZFS}^{B} = 1150 MHz, (b) D_{ZFS}^{A} = D_{ZFS}^{2B} = 2000 MHz, and (c) distribution of *D* as described in the text. The inserts are expansions of the top trace corresponding to a Gd-Gd distance of 8.3 nm.

Discussion

The Gd-rulers **1$_n$** and **2$_n$** (Figure 1) were designed as compounds for an in-depth evaluation of Gd(III) complexes as spin labels. Each compound consists of two Gd-PyMTA complexes that are connected via a rodlike spacer. The lengths of the spacers are strictly controlled by the synthesis and were chosen so as to obtain compounds with a Gd-Gd distance of 2 to 8 nm. The same spacer type had been used to connect two nitroxyl radicals (Figure 6) in order to obtain compounds for the methodological studies on EPR based distance determination.[6, 13, 48, 49, 52-55] From the results of DEER measurements on the nitroxyl-rulers the spacer's stiffness is well known.[6, 49, 55]

Therefore end-to-end distances are highly predictable, what makes the spacers ideal for studies of the type reported herein. To enable the DEER experiments with the Gd-rulers under the same conditions as applied to spin-labeled biomolecules, the spacers were furnished with branched oligoethylene glycol side chains. This gave compounds well soluble in the 7:3 (volume ratio) mixture of D_2O and glycerol-d_8, a solvent composition used for DEER measurements on proteins and also used throughout this study.

To evaluate the distance determination via Gd(III)-Gd(III) DEER measurements the Gd-Gd distances of the Gd-rulers $\mathbf{1_n}$ and $\mathbf{2_n}$, that were experimentally determined as described in the Results section, are compared to the expected distances (Figure 6). When calculating the expected Gd-Gd distances the bending of the rodlike spacers were taken into account through viewing the Gd-rulers as a cutout of a poly(*para*-phenyleneethynylene) chain, applying the wormlike chain model, and using the persistence length derived for this polymer in *ortho*-terphenyl from results of nitroxyl-nitroxyl DEER measurements on the nitroxyl-rulers $\mathbf{4_nref}$-$\mathbf{6_nref}$.[49] Additional data used for the calculation came from the X-ray structure analysis of Gd-ruler $\mathbf{1_1ref}$.[43] Details on the calculation are given in the Supporting Information. The calculation disregards that the side chains and solvents are quite different for the Gd-rulers and the nitroxyl-rulers. It is unknown whether these differences impact the spacer stiffness. The comparison in Figure 6 shows that the Gd-Gd distances determined from Gd(III)-Gd(III) DEER measurements at W and Q band agree very well with the expected distances. They deviate only up to 0.10 nm.

For the short Gd-rulers the maxima of the distance distributions at 1.9 nm and 2.9 nm are in good agreement with the expected distances of 2.1 and 3.0 nm. However, the distance distributions show spurious peaks at larger distances, which in practical terms are manifested as broadening or tailing of the distributions. As shown in the theoretical part this arises from neglecting the significant contribution of the pseudo-secular term in the dipolar Hamiltonian, i.e. the weak coupling approximation made when applying the DeerAnalysis software is not valid. The effect of the pseudo-secular term at distances of 3.4 nm and above is marginal and manifests itself primarily as a broadening of the DEER Pake pattern, which decreases with increasing distances. The consequence is a

broadening of the distance distribution obtained with software designed for the weak coupling case. As the minimal width at half height was found to be 0.4 nm, we can set this figure as an upper value for the broadening for distances above 3.4 nm.

The width of the distance distributions at half height for the Gd-rulers with a Gd-Gd distance of 3.4 nm and above is 0.4-0.7 nm and increases with the Gd-Gd distance (Table 1). The increase is assigned to an increase in bending amplitude when the spacer gets longer as was found for the analogous nitroxyl-rulers.[49] The width found for the Gd-rulers with Gd-Gd-distances of 2.9 nm and shorter has large contributions from neglecting the pseudo-secular term in the analysis and therefore cannot be used for any structural characterization. The shorter the distance is, the larger is the distortion.

In principle, one could develop an analysis procedure that does take into account the pseudo-secular term and thus could extract the correct distance distribution. This, however, requires the knowledge of the ZFS and its distribution thus making the extraction of the distance distribution complicated, lengthy and involving many parameters. Albeit the ZFS and its distribution can be determined for the parent Gd(III) complex, it is questionable whether these data are valid for the Gd(III) complex in applications, i.e. bound to a protein and therefore in a different environment. This will depend on the ligand used and especially on whether the coordination sphere of the Gd(III) ion is saturated or not. Additionally, in applications the Gd(III) complex will be bound to the protein via a tether with at least some conformational flexibility. This conformational flexibility generates an intrinsic distance distribution which will mask the broadening caused by neglecting the pseudo-secular term in the data analysis. Therefore one will get the expected distance as the absolute maximum of the distance distribution curve. This was shown in a recent work in which a distance of 2.4 nm was correctly determined.[27]

Our theoretical analysis predicts the effect of the pseudo-secular term due to overlap of the central transitions of the two Gd(III) ions to become stronger with decreasing ZFS. Accordingly, we expect that the effect will be stronger for Gd-DOTA based spin labels than for Gd-PyMTA based spin labels because Gd-DOTA has a smaller *D* value (~600 MHz)[22] than Gd-PyMTA (*D* ~1150, Figure 3). Accordingly, the latter should serve as a

better label for short distances. Because the width of the central transition is inversely proportional to the spectrometer frequency, it is expected that at Q band there will be less artifacts in the distance distribution curve and lower damping of the modulation depth than at W band. However, we did not find noticeable differences between the distance distributions obtained from Q- and W-band results. The major difference is in the SNR, which is better at W band.[56] This difference is expected due to the higher sensitivity achieved at higher fields, the associated decrease of the linewidth of the central transition leading to a larger λ, and the somewhat longer phase memory time. Our theoretical analysis also predicts that by avoiding detection or pumping at the |-3/2 >→ |-1/2> transition the effect of the pseudo-secular term can be minimized. This requires placing the observer pulses at the edges of the EPR spectrum (Figure 3). Such measurements, which require a non-resonant cavity with a huge bandwidth[15] or a dual mode cavity,[57] will be reported elsewhere.

Except for the short Gd-rulers $\mathbf{1_1}$ and $\mathbf{2_1}$, which exhibited the lowest modulation depth of 2.5-3% at W band, the samples exhibited a modulation depth of 3.5-4% when the pump pulse was set to the central transition. This is a relatively small deviation from the 5% obtained from homogenous frozen solutions of the parent complex, Gd-4-iodoPyMTA (**3**) (Figure S4). The smaller λ for the short distances is most probably associated with the overlap of the central transitions for the two Gd(III) ions within a pair. The theoretical approach presented in this work focuses on the frequency domain and therefore cannot account for effects on the modulation depth. Including this aspect would require full scale time domain calculations, which are currently underway.

Our results show that with Gd-PyMTA as a spin label, a Gd-Gd distance of 8.3 nm is easily accessible in solvents commonly used in studies on biomolecules. Moreover, for the concentration range of 0.02-0.05 mM in D_2O/glycerol-d_8 solutions DEER data can be collected up to 16 μs at 10K. Assuming that a minimum of one full modulation period is required for an unambiguous determination of the maximum of the distance distribution,[58] this evolution time defines the upper distance limit to 9.4 nm, it is 1 nm longer than what was measured in this work. Whether such long evolution times can be

obtained also with a protonated protein is yet to be seen. Even longer distances should be accessible with the 5 pulse DEER sequence.[59]

It has been recently shown that Gd(III)-nitroxyl DEER measurements at Q and W band is yet another attractive approach for distance determination.[38, 39, 41] In this case the effect of the pseudo-secular term should pose less of a problem, because the overlap between the nitroxyl radical transition and the Gd(III) transitions is limited to the broad background of the Gd(III) spectrum, attributed to transitions other than the central one. A theoretical analysis that takes into account the ZFS for such measurements has been reported.[38]

Conclusions

A series of Gd-rulers with well-defined Gd-Gd distances in the range of 2.1-8.5 nm (expected distances) and Gd-PyMTA as the spin label was used to evaluate the Gd-Gd distance determination through Gd(III)-Gd(III) DEER measurement at W and Q band in combination with data analysis using the standard DeerAnalysis program. Data analysis with the standard DeerAnalysis program means that the Gd(III)-Gd(III) pair is treated like a pair of weakly coupling spins with S = 1/2 despite of the difference in S and despite of the ZFS of Gd(III) ions. A very good agreement between the expected distances and the distances corresponding to the absolute maxima of the experimentally determined distance distribution curves was obtained at both frequencies for distances of 3.4 nm and larger. Even at distances of 2.9 nm and 2.1 nm the agreement is very good. However, the experimentally determined distance distribution curves contain in addition to the main peak spurious peaks, that can be mistaken as giving evidence of the presence of other species or of additional conformations of the molecule under study. Theoretical analysis traces back these peaks to disregarding the pseudo-secular term when applying an analysis tool designed for a pair of spins with S = 1/2. The effect of the pseudo-secular term is well manifested in the Fourier transform spectra of the DEER traces: For Gd-Gd distances of 1.9 and 2.9 nm the pseudo-secular term causes severe deviations of the spectrum from a Pake pattern, whereas for distances of 3.4 nm and above it causes broadening of the spectra that decreases with increasing distance. This extra broadening will be translated into a

broadening of the distance distribution. The minimal width at half height obtained experimentally was about 0.4 nm. Considering that most DEER measurements are applied to biomolecules with an inherent flexibility of the tether connecting the Gd(III) ion and the point of attachment at the biomolecule this broadening is expected to be not of concern for most applications. The long phase memory time of 16 µs found for D_2O/glycerol-d_8 solutions at 10 K suggests that with four-pulse DEER distances up to 9.4 nm can be accessed with Gd-PyMTA as the spin label.

The effect of the dipolar pseudo-secular term scales with the size of the ZFS and gets smaller with increasing *D* values. Therefore, it is the large distribution of *D* of Gd(III) complexes in a frozen solution that enables the Gd(III) complexes to be used as spin labels for distance measurements at Q band and higher fields. Furthermore, it clearly points out the need for ligand design to adjust the ZFS parameters. E.g. Gd-PyMTA is better suited for short distances than Gd-DOTA.

The study demonstrates the merits of working with a series of geometrically well-defined model compounds and outlines the way how to study the suitability and limits of other Gd(III) complexes as well as of other EPR techniques targeting Gd(III) complexes as a spin label.

Acknowledgments

We thank G. Jeschke for helpful discussion and M. Hülsmann for contributions to the synthesis. For the syntheses of the Gd-rulers funding from the DFG priority program SPP 1601 (grant GO 555/6-1) is acknowledged. This work was also supported by the Israel-USA BSF science foundation (D.G.). This research was also made possible in part by the historic generosity of the Harold Perlman Family. D. G. holds the Erich Klieger professorial chair in Chemical Physics.

Supporting Information available.

Experimental details of the DEER measurements, samples details, pulse length optimization, additional echo decay data, DEER background decay measurements on

Gd-4-iodo-PyMTA, W-band primary DEER data, additional W-band DEER data of Gd-ruler $\mathbf{1_9}$, Q-band primary DEER data, Q-band Gd-Gd dipolar simulations, calculation of the expected distances.

References

1. G. Jeschke, in *Structural Information from Spin-Labels and Intrinsic Paramagnetic Centres in the Biosciences*, eds. C. R. Timmel and J. R. Harmer, Springer Berlin Heidelberg, 2013, vol. 152, ch. 61, pp. 83-120.
2. O. Schiemann and T. F. Prisner, *Quaternary Rev. Biophys.*, 2007, **40**, 1-53.
3. P. P. Borbat and J. H. Freed *Struct. Bond.*, 2013, **152**, 1-82.
4. M. Drescher and G. Jeschke, eds., *EPR Spectroscopy: Applications in Chemistry and Biology* Springer, 2012.
5. Y. W. Chiang, P. P. Borbat and J. H. Freed, *J. Magn. Reson.*, 2005, **172**, 279-295.
6. G. Jeschke, V. Chechik, P. Ionita, A. Godt, H. Zimmermann, J. Banham, C. R. Timmel, D. Hilger and H. Jung, *Appl. Magn. Reson.*, 2006, **30**, 473-498.
7. W. L. Hubbell and C. Altenbach, *Curr. Opin. Struct. Biol.*, 1994, **4**, 566-573.
8. O. Duss, M. Yulikov, G. Jeschke and F. H. T. Allain, *Nat. Comm.*, 2014, **5**.
9. S. A. Shelke and S. T. Sigurdsson, *Struct. Bond.*, 2013, **152**, 121-162.
10. J. P. Klare and H.-J. Steinhoff, *Photosynth. Res.*, 2009, **102**, 377-390.
11. T. J. Stone, T. Buckman, P. L. Nordio and H. M. McConnel, *Proc. Nat. Acad. Sci.USA*, 1965, **54**, 1010-1017.
12. H. Ghimire, R. M. McCarrick, D. E. Budil and G. A. Lorigan, *Biochemistry*, 2009, **48**, 5782-5784.
13. Y. Polyhach, E. Bordignon, R. Tschaggelar, S. Gandra, A. Godt and G. Jeschke, *Phys. Chem. Chem. Phys.*, 2012, **14**, 10762-10773.
14. P. Zou and H. S. McHaourab, *Biophys. J.*, 2010, **98**, L18-L20.
15. P. A. S. Cruickshank, D. R. Bolton, D. A. Robertson, R. I. Hunter, R. J. Wylde and G. M. Smith, *Rev. Sci. Instrum.*, 2009, **80**, 103102.
16. D. Goldfarb, Y. Lipkin, A. Potapov, Y. Gorodetsky, B. Epel, A. M. Raitsimring, M. Radoul and I. Kaminker, *J. Magn. Reson.*, 2008, **194**, 8-15.
17. Y. Polyhach, A. Godt, C. Bauer and G. Jeschke, *J. Magn. Reson.*, 2007, **185**, 118-129.
18. I. Tkach, S. Pornsuwan, C. Hoebartner, F. Wachowius, S. T. Sigurdsson, T. Y. Baranova, U. Diederichsen, G. Sicoli and M. Bennati, *Phys. Chem. Chem. Phys.*, 2013, **15**, 3433-3437.
19. Z. Yang, Y. Liu, P. Borbat, J. Zweier, J. Freed and W. Hubbell, *Biophys. J.*, 2012, **102**, 405A-405A.
20. G. Y. Shevelev, O. A. Krumkacheva, A. A. Lomzov, A. A. Kuzhelev, O. Y. Rogozhnikova, D. V. Trukhin, T. I. Troitskaya, V. M. Tormyshev, M. V. Fedin, D. V. Pyshnyi and E. G. Bagryanskaya, *J. Am. Chem. Soc.*, 2014, **136**, 9874-9877.
21. D. Goldfarb, *Phys. Chem. Chem. Phys.*, 2014, **16**, 9685-9699.
22. A. M. Raitsimring, C. Gunanathan, A. Potapov, I. Efremenko, J. M. L. Martin, D. Milstein and D. Goldfarb, *J. Am. Chem. Soc.*, 2007, **129**, 14138-14140.
23. A. Potapov, Y. Song, T. J. Meade, D. Goldfarb, A. V. Astashkin and A. Raitsimring, *J. Magn. Reson.*, 2010, **205**, 38-49.
24. Y. Song, T. J. Meade, A. V. Astashkin, E. L. Klein, J. H. Enemark and A. Raitsimring, *J. Magn. Reson.*, 2011, **210.** 59-68.
25. H. Yagi, D. Banerjee, B. Graham, T. Huber, D. Goldfarb and O. Gottfried, *J. Am. Chem. Soc.*, 2011, **133**, 10418-10421.

26. A. Potapov, H. Yagi, T. Huber, S. Jergic, N. E. Dixon, G. Otting and D. Goldfarb, *J. Am. Chem. Soc.*, 2010, **132**, 9040-9048.
27. Devin T. Edwards, T. Huber, S. Hussain, Katherine M. Stone, M. Kinnebrew, I. Kaminker, E. Matalon, Mark S. Sherwin, D. Goldfarb and S. Han, *Structure*, 2014, **22**, 1677-1686.
28. M. Gordon – Grossman, I. Kaminker, Y. Gofman, Y. Shai and D. Goldfarb, *Phys. Chem. Chem. Phys.*, 2011, **13**, 10771-10780.
29. E. Matalon, T. Huber, G. Hagelueken, B. Graham, A. Feintuch, V. Frydman, G. Otting and D. Goldfarb, *Angew. Chem. Int. Ed.*, 2013, **52** 11831-11834
30. M. Yulikov, P. Lueders, M. F. Warsi, V. Chechik and G. Jeschke, *Phys. Chem. Chem. Phys.*, 2012, **14**, 10732-10746.
31. B. G. Martorana A., Feintuch A., Di Gregorio E., Aime S., Goldfarb D., *J. Am. Chem. Soc.* , 2014, **136,** 13458-13465.
32. M. Qi, A. Gross, G. Jeschke, A. Godt and M. Drescher, *J. Am. Chem. Soc.*, 2014, **136**, 15366-15378.
33. I. Krstic, R. Haensel, O. Romainczyk, J. W. Engels, V. Doetsch and T. F. Prisner, *Angew. Chem. Intl. Ed.*, 2011, **50**, 5070-5074.
34. M. Azarkh, O. Okle, V. Singh, I. T. Seemann, J. S. Hartig, D. R. Dietrich and M. Drescher, *Chembiochem*, 2011, **12**, 1992-1995.
35. M. Azarkh, V. Singh, O. Okle, D. R. Dietrich, J. S. Hartig and M. Drescher, *Chemphyschem*, 2012, **13**, 1444-1447.
36. A. Doll, M. Qi, S. Pribitzer, N. Wili, M. Yulikov, A. Godt and G. Jeschke, *Phys. Chem. Chem. Phys.*, 2015, **17**, 7334-7344.
37. S. Razzaghi, M. Qi , Nalepa A. I., A. Godt, G. Jeschke , S. Anton and Y. Maxim, *J. Phys. Chem. Lett.*, 2014, **5**, 3970–3975.
38. P. Lueders, G. Jeschke and M. Yulikov, *J. Phys. Chem. Lett.*, 2011, **2**, 604-609.
39. I. Kaminker, H. Yagi, T. Huber, A. Feintuch, G. Otting and D. Goldfarb, *Phys. Chem. Chem. Phys.*, 2012, **14**, 4355-4358.
40. P. Lueders, H. Jager, M. A. Hemminga, G. Jeschke and M. Yulikov, *J. Phys. Chem. B*, 2013, **117**, 2061-2068.
41. I. Kaminker, I. Tkach, N. Manukovsky, T. Huber, H. Yagi, G. Otting, M. Bennati and D. Goldfarb, *J. Magn. Reson.*, 2013, **227**, 66-71.
42. L. Garbuio, E. Bordignon, E. K. Brooks, W. L. Hubbell, G. Jeschke and M. Yulikov, *J. Phys. Chem. B*, 2013, **117**, 3145-3153.
43. C. Gunanathan, Y. Diskin-Posner and D. Milstein, *Crystal Growth & Design*, 2010, **10**, 4235-4239.
44. D. Goldfarb, ed., *Metal-Based Spin Labeling for Distance Determination*, Springer-Verlag Berlin Heidelberg 2012.
45. A. Raitsimring, A. Dalaloyan, A. Collauto, A. Feintuch, T. Meade and D. Goldfarb, *J. Magn. Reson.*, 2014, **248**, 71-80.
46. S. Stoll and A. Schweiger, *J. Magn. Reson.*, 2006, **178**, 42-55.
47. A. M. Raitsimring, A. V. Astashkin, O. G. Poluektov and P. Caravan, *Appl. Magn. Reson.*, 2005, **28**, 281-295.
48. M. Pannier, S. Veit, A. Godt, G. Jeschke and H. W. Spiess, *J. Magn. Reson.*, 2000, **142**, 331-340.
49. G. Jeschke, M. Sajid, M. Schulte, N. Ramezanian, A. Volkov, H. Zimmermann and A. Godt, *J. Am. Chem. Soc.*, 2010, **132**, 10107-10117.
50. W. Low, *Solid State Physics*, Academic Press, New York, 1960.
51. A. Borel, H. Kang, C. Gateau, M. Mazzanti, R. B. Clarkson and R. L. Belford, *J. Phys. Chem. A*, 2006, **110**, 12434-12438.
52. G. Jeschke, M. Sajid, M. Schulte and A. Godt, *Phys. Chem. Chem. Phys.*, 2009, **11**, 6580-6591.

53. G. W. Reginsson, R. I. Hunter, P. A. S. Cruickshank, D. R. Bolton, S. T. Sigurdsson, G. M. Smith and O. Schiemann, *J. Magn. Reson.*, 2012, **216**, 175-182.
54. N. C. Kunjir, G. W. Reginsson, O. Schiemann and S. T. Sigurdsson, *Phys. Chem. Chem. Phys.*, 2013, **15**, 19673-19685.
55. A. Godt, M. Schulte, H. Zimmermann and G. Jeschke, *Angew. Chem. Int. Ed.*, 2006, **45**, 7560-7564.
56. A. Raitsimring, A. V. Astashkin, J. H. Enemark, I. Kaminker, D. Goldfarb, E. D. Walter, Y. Song and T. J. Meade, *Appl. Magn. Reson.*, 2013, **44**, 649-670.
57. I. Tkach, G. Sicoli, C. Höbartner and M. Bennati, *J. Magn. Reson.*, 2011, **209**, 341-346.
58. G. Jeschke and Y. Polyhach, *Phys. Chem. Chem. Phys.*, 2007, **9**, 1895-1910.
59. P. P. Borbat, E. R. Georgieva and J. H. Freed, *J. Phys. Chem. Lett.*, 2013, **4**, 170-175.

Table of content graphic (TOC)